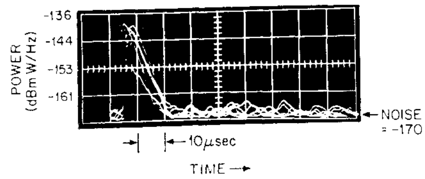

Fig. 3 PPT RFI measurements.

wave. Waves at λ_0 incident at an angle with respect to the normal, have only the normal component completely absorbed. For the PPT, RFI experiments, a significant portion of the radiated wave was not normal to the absorber and some ringing took place within the cavity formed by the vacuum tank walls. This ringing was due to the presence of high-order coaxial modes propagating parallel to the absorber sheet. RFI measurements were made initially on a PPT mounted in the flight configuration with respect to the antennas. The results of the experiment were in error for the chamber acted as an echo box to yield erroneous time duration RFI measurements.

Two successive experiments were subsequently performed. One used a vacuum bell jar to house the PPT and a monopole antenna cut for 300 MHz ($VSWR = 1.35{:}1$) mounted both inside and outside the jar. The walls of the measurement area were lined with the broadband absorber blocks of the type used in large anechoic chambers to prevent reflections of the rf energy. The effects of antenna coupling were proved to be small in this experiment for the amplitude of the RFI was essentially independent of antenna location. Finally, RFI measurements were made in a 4 ft diam vacuum tank completely lined with broadband ferrite absorber material.‡ This environment rendered measurements free from any chamber resonance effects. Measurements were made of RFI time duration above the measurement threshold as seen in a 100 kHz bandwidth. The amplitude results of the three experiments agreed to within a few db/Hz and the time duration results varied from 40 μsec in the first experiment§ to 10–15 μsec in the last experiment. Although there were some uncertainties in the discharge time of the thruster, it was expected to be more in the neighborhood of 2–3 μsec rather than 10–15 μsec. This additional stretching is attributed to the (relatively) narrow bandwidth of observation. The answers, nonetheless, were sufficient for the LES-6 purposes. Figure 3 gives the RFI power vs time recorded from measurements on five successive firings in the 4-ft-diam ferrite lined chamber. The center frequency was 300 MHz and the Bandwidth 100 kHz. The peak power varied from −139 dBmw/Hz to −149 dBmw/Hz with successive firings of the plasma thruster.

Conclusions

A technique has been evolved to measure RFI emanating from a Pulse Plasma Thruster. This involves the measurement of the amount of r.f. power received at an antenna having a plasma in the near field. It is desirable to make the measurement in a vacuum anechoic chamber with the plasma and receiving antenna in their flight orientation. If this is not possible a good estimation of the RFI power may be obtained by using smaller vacuum anechoic chambers of low electrical Q to house the PPT and a test antenna.

Reference

[1] Guman, W. J. and Nathanson, D. M., "Pulsed Microthruster Propulsion System for Synchronus Orbit Satellite," *Journal of Spacecraft and Rockets*, submitted for publication.

‡ Typically 15 db return loss from 50 MHz to 15 GHz.

§ The additional 25–30 μsec duration due to ringing.

Generalized One-Dimensional, Compound Compressible Nozzle Flow

David J. Norton*
Jet Propulsion Laboratory, Pasadena, Calif.

Nomenclature

A	= area
a,b	= constants, b/ρ_P and r/P^n, respectively
C	= constant for perfect gas
$E = E(\psi)$	= energy of a streamline
H_0,h	= stagnation and static enthalpy, respectively
$\Delta H_c,\Delta H_v$	= heats of combustion and vaporization, respectively
K	= flow coefficient, constant
$\mathfrak{M}$	= molecular weight
$\dot{m}$	= mass flow rate
O/F	= oxidizer/fuel flow ratio
P	= pressure
r	= radial coordinate, or burning rate
R	= radius
R_g	= perfect gas constant
T	= temperature
U,V,W	= radial, tangential, and axial velocities, respectively
ϵ_c	= contraction ratio, A_c/A_t
γ	= specific heat ratio
$\Gamma = \Gamma(\Psi)$	= $V \times r$
Ψ	= stream function $= \int_0^{\dot{m}(r)} \frac{d\dot{m}}{\dot{m}_T}$
ω	= angular velocity
ρ	= density

Subscripts

0	= stagnation condition
1,2	= inner and outer zones, respectively
c,cl,I	= chamber, centerline, and injector, respectively
f,g,L,P	= flame gas, liquid, and propellant, respectively
R,T,t,w	= reservoir, total, throat, and wall, respectively

Introduction

THERE are occasions in the design of nozzles when it is convenient to treat flows in which the entropy (i.e., total pressure, total temperature) varies normal to the streamlines but is conserved along the streamlines. In the case when two-dimensional effects are of secondary importance, the flows from rotating rocket motors or bypass turbojet engines, for example, can be treated by special one-dimensional techniques. Some of the ground work has been laid for such analyses.[1–4] This paper describes a unified theory for which the specific problems listed earlier are subsets and presents specific examples of its uses.

Analysis

The properties of the flowfield are assumed to be known at the nozzle inlet (see Fig. 1a). It is desired to evaluate the radial distribution of the flow variables at the throat plane and to determine the radius, R_t, required to choke the flow as defined by the initial conditions. The following restrictions (some of which can be removed as discussed later) are placed on the flow for the flow for the initial develop-

Received September 24, 1969; revision received October 31, 1969. This paper presents the results of one phase of research carried out at the Jet Propulsion Laboratory, California Institute of Technology, under NASA Contract NAS 7-100.

* Captain, U.S. Army; Senior Engineer, Jet Propulsion Laboratory; presently Aerospace Engineering Department, Texas A & M University, College Station, Texas. Member AIAA.

ment: the flow is steady, adiabatic, and inviscid; the gas associated with each streamline is thermally and calorically perfect; and radial velocities are negligibly small. Under these restrictions the equations for axisymmetric flow are, normal to streamlines;

$$d\dot{m} = 2\pi\rho Wrdr,\ dP = \rho\{[\Gamma(\Psi)]^2/r^3\}dr \quad (1)$$

Along streamlines;

$$\Gamma = \Gamma_{(\Psi)};\quad P = \rho^\gamma C(\Psi);\quad E = E(\Psi) \quad (2)$$

In general, γ, $\mathfrak{M}$, T_0, P_0, and Γ vary with each streamline, and they are determined by the initial chamber conditions. By substituting Eqs. (2) into Eqs. (1) the governing equations can be reduced to two nonlinear, simultaneous differential equations,

$$W = \pm\left[2\left(E - \frac{\gamma}{\gamma - 1}\, C^{1/\gamma}\, P^{(\gamma-1)/\gamma}\right) - \frac{\Gamma^2}{r^2}\right]^{1/2} \quad (3)$$

Therefore,

$$d\dot{m} = \pm\, 2\pi\left(\frac{P}{C}\right)^{1/\gamma} \times \left[2\left(E - \frac{\gamma}{\gamma - 1}\, C^{1/\gamma}\, P^{(\gamma-1)/\gamma}\right) - \frac{\Gamma^2}{r^2}\right]^{1/2} rdr \quad (4)$$

$$dP = (P/C)^{1/\gamma}(\Gamma^2/r^3)dr \quad (5)$$

Equations (5) and (6) are the general governing equations, the boundary conditions for which are

$$\left.\begin{array}{l} r = r_i,\ \dot{m} = 0, \quad P = P_{cl} \\ r = r_w,\ \dot{m} = \dot{m}_T,\ P = P_w \end{array}\right\} \quad (6)$$

In most cases $r_i = 0$; however, if a centerbody is present, integration should be initiated at this boundary. Equations (4) and (5) are solved in a plane defined by a P_{cl}. The plane of most interest is the plane of minimum cross-sectional area (A_t). For flows with a centerbody, some care must be taken to identify this plane. The best method is provided by a calculus of variations approach. Since there is no general criterion for the P_{cl} yielding A_t for compound flows, the selection of the P_{cl} at the physical throat is accomplished iteratively. For each pressure selected Eqs. (4) and (5) are integrated observing the distribution of $\mathfrak{M}$, γ, E, C, and Γ with Ψ as determined by a solution for the particular chamber conditions. The chamber solution depends upon the method of mass generation and the properties of the combustion products. The chamber solution then determines the flow properties at the nozzle inlet. It is not necessary to introduce any artificial choking criteria to obtain the R_t, but to obtain a particular desired design value, one must alter the gas static pressure at the nozzle inlet, P_g or an equivalent parameter and recalculate the nozzle inlet conditions. Thus, a solution can be obtained which simultaneously satisfies the chamber and throat requirements, by employing a double iterative method. It is possible to consider rotational flows in which entropy varies from streamline to streamline, as well as problems which include axisymmetric centerbodies.

Table 1 Results for LOX-hydrazine[a] with fuel-rich injection at wall[b]

Chamber condition	$\epsilon_c = 2$ Zone 1	$\epsilon_c = 2$ Zone 2	$\epsilon_c = 9$ Zone 1	$\epsilon_c = 9$ Zone 2
P_t, psia	118.6		112.0	
P_L, psia	223.4		200.9	
P_o, psia	212.26	212.34	200.52	200.53
T_o, °R	5830	3539	5830	2539
T_g, °R	5795	3508	5826	3538
W_g, fps	1324	1251	279.0	264.6
A_g/A_c	0.801	0.199	0.801	0.199
M_t	1.0037	0.9837	1.0037	0.9837

[a] $W_I = 30$ fps liquid injection velocity.
$_2/\dot{m}_T\, q = 0.20$, $P_g = 200$ psia, $0/F_1 = 1$, $\gamma_1 = 1.219$, $\mathfrak{M}_1 = 19.66$, $0/F_2 = 0.25$, $\gamma_2 = 1.285$, and $\mathfrak{M}_2 = 13.35$.

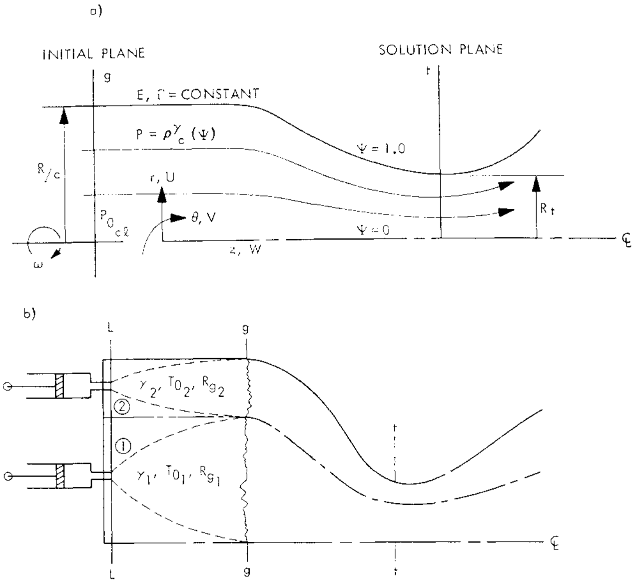

Fig. 1 The model for the inviscid theory of rotating flow in nozzles, and schematic of the injector and nozzle flowfields; with constant-displacement injectors.

For nonrotating flows, considerable simplification in the governing equation can be achieved, since $dP/dr = 0$, $\Gamma = 0$, and Eq. (4) applies without the Γ^2/r^2 term.

For irrotational vortex flows, Γ is constant for all Ψ, as for internal-burning solid-propellant grains; $\Gamma = V_wR_w = K$. Since the flowfield is also homentropic, C and E are constants for all streamlines. In Eqs. (4) and (5), Γ^2 is replaced by K^2. Integration must start from the edge of the void region ($r \neq 0$, $\dot{m} = 0$, $P = 0$).[1,5,6]

For rotational vortex flow, $\Gamma = r^2\omega = \Gamma(\Psi)$ at the propellant face in an end-burning motor, and Eqs. (4) and (5) apply. Integration can start from $r = 0$; however, it may be necessary to consider the negative sign in Eq. (4) to account for reverse core flow.[1,5,7]

For flows in which a discrete number of zones are considered, it is possible to reduce the differential equations to algebraic equations, which are solved by iterating on P until R_n is minimized,

$$\dot{m}_i = \pm\pi\left(\frac{P}{C_i}\right)^{1/\gamma_i} 2\left(E_i - \frac{\gamma_i}{\gamma_{i-1}}\, C_i^{1/\gamma_i}P^{\gamma_i - 1/\gamma_i}\right)^{1/2} \times (R_i^2 - R_{i-1}^2) \quad (7)$$

$$\dot{m}_0 = \sum_{i=1}^{n} \dot{m}_i \quad (8)$$

Constant-displacement injectors ($\dot{m}$ = constant)

Figure 1b illustrates the use of constant $-\dot{m}$ injectors. Two zones ($i = 1,2$) are considered, the interior zone ($i = 1$) at high T_f and the outer zone ($i = 2$) with fuel-rich injection. The energy, momentum, and mass equations for each zone are

$$h_{Li} + W_{Li}^2/2 + \Delta H_{ci} + \Delta H_{vi} = H_{0gi} = h_{gi} + W_{gi}^2/2 \quad (9)$$

$$A_{gi}P_{Li} + \rho_{Li}W_{Li}^2A_{Ii} = P_{gi}A_{gi}\, 1 + \frac{W_{gi}^2}{R_{gi}T_{gi}} \quad (10)$$

$$\rho_{Li}W_{Li}A_{Ii} = \dot{m}_i = \rho_{gi}W_{gi}A_{gi} \quad (11)$$

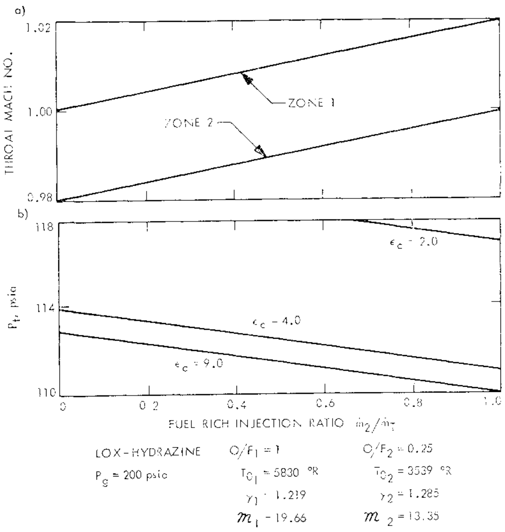

Fig. 2 Throat Mach number and pressure for a two-zone flow with constant displacement injectors.

Since $V = 0$ and $U \cong 0$,

$$P_{L1} = P_{L2}; \quad P_{g1} = P_{g2}; \quad A_c = A_{g1} + A_{g2} \tag{12}$$

Equations (9–12) give a system of eight equations for which there are eight unknowns: T_{g1}, T_{g2}, W_{g1}, W_{g2}, A_{g1}, A_{g2}, P_{L1}, and P_{L2}. Therefore, there exists a solution for the chamber properties for an assumed P_g. In a practical case, the energy equations are solved employing a chemical reaction computer program for the desired O/F in each zone, and R_t is determined by applying Eqs. (7) and (8) for various P_{cl} until R_t is minimized. It may be necessary to adjust P_g until Eqs. (7) and (8) give the desired throat value.

Table 1 presents some results for a LOX-hydrazine, P_g = 200 psia system in which fuel-rich injection was employed at the walls. For this case 20% of the total flow was specified to have $(O/F)_2 = 0.25$, yielding an equilibrium T_f of 3539°R, while $(O/F)_1 = 1.00$, yielding 5830°R. Chamber conditions are presented for two ϵ_c; these results indicate that there can be significant differences in P_0 and W_g for the two zones even when P_g is uniform. These results further show that P_L may not be assumed equal to P_g when calculating $\dot m_I$, especially at low contraction ratios.

Figure 2a shows that M_t is uniformly unity only at $\dot m_2/\dot m_T = 0$, and $\dot m_1/\dot m_T = 1$. Figure 2b presents P_t vs $\dot m_2/\dot m_T$ for three ϵ_c; the variation of P_t with $\dot m_2/\dot m_T$ is due to changing effective γ and $\mathfrak{M}$ for the gases.

Constant-pressure-reservoir injection P_R = constant

When the chamber is fed propellants from constant $-P_R$ reservoir, an increase in P_g (hence, decrease in $P_R - P_L$) results in a decrease of $\dot m$. The physical model for this case is similar to Fig. 1b except that the constant $\dot m$ injectors are replaced by a reservoir at a fixed P_R. In practice it is often desirable to maintain a fixed P_R/P_L to assure a "stiff" injection system. If we define $X_i = (P_R/P_L)_i - 1$, then

$$\dot m_i = A_{I_i} K_i (2\rho_{Li} P_L X_i)^{1/2} \tag{13}$$

Use of Eq. (13) with Eqs. (9–12) is then sufficient to determine the chamber conditions.

Figure 3 presents some results for constant $\dot m$ and constant P_R injectors for a range of ϵ_c for a LOX-H_2 motor in which $(O/F)_1 = 8$ and $(O/F)_2 = 3$. These conditions provided $T_{f1} = 6081$°R and $T_{f2} = 3292$°R. For the constant $\dot m$ injectors, $\dot m_1/\dot m_T = 0.20$, and the constant $-P_R$ case, was $A_{I2}/A_{IT} = 0.20$. The two motors operate along different $P_g(\epsilon_c)$ curves; however, when the P_g of the two motors are equal, the $\dot m$ also agree.

Rotating, solid-propellant, end-burning motor

In a solid-propellant motor, $\dot m \propto P^n$; this effect is of particular importance in rotating motors, where the tangential velocity tends to decrease the effective throat size of the nozzle.[1,5,8,9] Let us consider an end-burning rocket motor rotating at a specified ω with a given P_{cl} at the propellant surface

$$T_0 = T + (V^2 + W^2)/2C_P \tag{14}$$

Referring to Fig. 1a, the rotating burning surface is assumed to be at g, where the streamlines emanating from that surface possess a component of angular velocity. For the combustion gases leaving the propellant surface, T_0 is related to the T_f of the propellant and the kinetic energy due to the radial distribution tangential velocity component of the spinning grain:

$$T_0 = T_f + V^2/2C_P \tag{15}$$

Since, $W = aR_gTP^{n-1}$, it may be expressed as,

$$T_f = T + (aR_gTP^{n-1})^2/2C_P \tag{16}$$

which, when solved for pressure, yields

$$P = [2(T_f - T)C_P/(aR_GT)^2]^{1/2(n-1)} \tag{17}$$

To solve explicitly for $T(r)$ or $P(r)$, it is necessary to employ the radial momentum equation

$$dP/\rho = [R_gT(dP/P)] = (V^2/r)dr = (\omega^2 r dr) \tag{18}$$

where the latter parenthetic equality applies because the

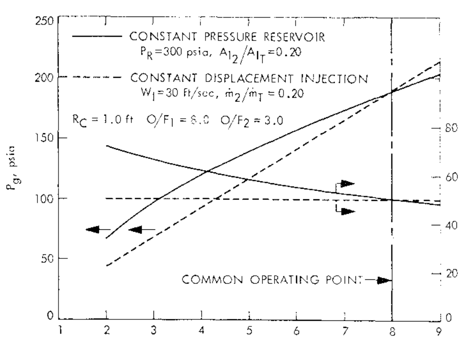

Fig. 3 Operating characteristics for LOX-H2 motors with two injection techniques.

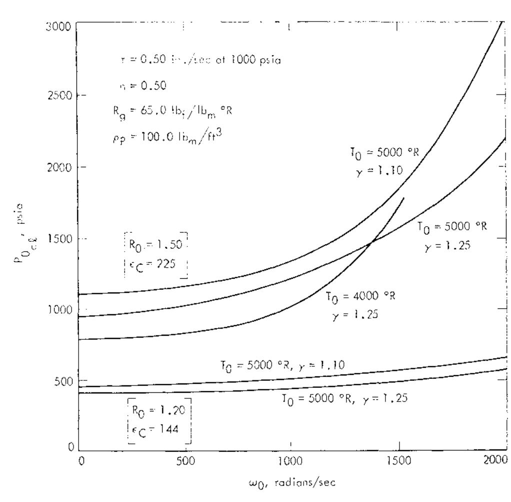

Fig. 4 Chamber pressure vs rate of rotation for end-burning motors with various propellant properties.

propellant surface rotates as a solid body. Hence

$$\int_0^r T\frac{dP}{P} = \frac{\omega^2 r^2}{2R_g} \tag{19}$$

Using Eq. (17), the left side of Eq. (19) can be expressed as a function of temperature only,

$$T\frac{dP}{P} = \left(\frac{1}{2n-2}\right)\left[\frac{-2T_f T^{-2} + T^{-1}}{T_f T^{-2} - T^{-1}}\right]dT \tag{20}$$

Substituting Eq. (18) into Eq. (17) and multiplying each side by T^2 allows the left side of Eq. (20) to be integrated where $T^* = T/T_f$

$$T^* = \ln\left(\frac{1-T^*}{1-T_{cl}^*}\right) + \frac{\omega^2 r^2(1-n)}{T_f R_g} + T_{cl}^* \tag{21}$$

It can be shown that T^* must lie between T_{cl}^* and 1.0. Once $T^*(r)$ is obtained, the radial momentum Eq. (17) can be integrated to obtain $P(r)$. The integration can be carried out numerically from the specified P_{cl} to the desired $P(r)$

$$P(r) = P_{cl}\exp\left[\frac{\omega^2}{R_g}\int_0^r \frac{rdr}{T(r)}\right] \tag{22}$$

The properties across the propellant surface can be evaluated by substituting the $T^*(r)$ from Eq. (21) and the $P(r)$ from Eq. (22) into Eqs. (1), (14), $W = aR_gTP^{n-1}$, and $P_0 = P(T_0/T)^{\cdot\gamma/(\gamma-1)}$. In addition, the functions relating the properties along the streamlines may be evaluated at the propellant surface:

$$C(\Psi) = [R_gT_0(\Psi)]^\gamma/P_0(\Psi)^{\gamma-1} \tag{23}$$

$$E = H_0(\Psi);\quad \Gamma = \omega r^2 \tag{24}$$

Figure 4 presents some typical results for the variation of P_{ocl} with ω for end-burning motors. As ω is increased for a given P_{ocl}, the throat size required to pass the same mass flow also increases. In most cases it is desired to find the chamber conditions which will occur for a particular ω and ϵ_c. Under these circumstances, it is necessary to vary the P_g at a given ω until the desired R_t is obtained. Increasing ϵ_c, or decreasing T_f or γ, increases the pressure sensitivity of the propellant to rotation. These effects can be explained qualitatively in the following manner. Decreasing γ or T_f tends to decrease the sonic velocity of the gas, hence W_t is reduced. Increasing ϵ_c tends to increase the tangential V_t due to the conservation of angular momentum. Thus for a given ω, V_t/W_t becomes larger for increasing contraction ratio and decreasing γ and T_f of the propellant gases. As V_t increases, the effective A_t decreases. An increase in $\mathfrak{M}$ affects P_g in the same manner as a decrease in T_f or γ.

Concluding Remarks

The theory presented here permits the extension of one-dimensional flow concepts to flows which are not homentropic and homoenergetic. The solution for a particular problem depends upon the initial conditions and the nozzle geometry. Once the throat is determined, other planes in the subsonic and supersonic portions of the nozzle can be investigated, recalling that radial velocities are assumed to be negligibly small.

The effects of changing composition along a streamline may be included in a simple manner if equilibrium reactions are assumed to occur. In this case, a map of the molecular weight $\mathfrak{M}$, specific heat ratio γ, and temperature T as a function of pressure should be determined. Then, during the iteration for the throat pressure, the correct values of γ, $\mathfrak{M}$, and T can be introduced for each stream tube as determined by equilibrium calculations for the assumed pressure. The problem of flow with chemical kinetics may also be studied; however, a time integration must be made reflecting the proper nozzle geometry.

References

[1] Norton, D. J., Farquhar, B. W., and Hoffman, J. D., "An Analytical and Experimental Investigation of Swirling Flow in Nozzles," *AIAA Journal*, Vol. 7, No. 10, Oct. 1969, pp. 1992–2000.

[2] Bernstein, A., Heiser, W., and Hevenor, C., "Compound-Compressible Nozzle Flows," *Transactions of the ASME*, Sept. 1967, pp. 548–554.

[3] Pearson, H. et al, "A Theory of the Cylindrical Ejector Supersonic Propelling Nozzle," *Journal of the Royal Aeronautical Society*, London, Sec. 62, 1958, pp. 746–751.

[4] Hodge, H. J. and Segars, R. A., "Choked Flow: A Generalization of the Concept and Some Experimental Data," *AIAA Journal*, Vol. 3, No. 12, Dec. 1965, pp. 2177–2183.

[5] Norton, D. J., Farquhar, B. W., and Hoffman, J. D., "Analytical Studies of the Interior Ballistics of Spin Stabilized Rocket Motors—A Literature Survey," Rept. TM-67-1, Jan. 1967, Jet Propulsion Center, Purdue Univ.

[6] Mager, A., "Approximate Solution of Isentropic Swirling Flow Through a Nozzle," *ARS Journal*, Vol. 31, Aug. 1961, pp. 1140–1148.

[7] Lewellen, W. S., Burns, W. J., and Strickland, H. J., "Transonic Swirling Flow," *AIAA Journal*, Vol. 7, No. 7, July 1969, pp. 1290–1297.

[8] Bastress, E. K., "Interior Ballistics of Spinning Solid Propellant Rockets," *Journal of Spacecraft and Rockets*, Vol. 2, No. 3, May-June 1965, pp. 455–457.

[9] Manda, L., "Spin Effects on Rocket Nozzle Performance," *Journal of Spacecraft and Rockets*, Vol. 3, No. 11, Nov. 1966, pp. 1695–1696.

[10] B. W. Farquhar, private communication, April 1969, Boeing Co., Renton, Wash.

Reaction between Oxygen Difluoride and Diborane. I: Preliminary Results

ROBERT A. RHEIN*
Jet Propulsion Laboratory, Pasadena, Calif.

Introduction

MISSION studies[1] have indicated that the OF_2—B_2H_6 propellant system, with a calculated maximum specific impulse (1000–14.7 psi) of 368 sec, can provide a payload capability exceeding that of F_2—H_2 and O_2—H_2 and that it has advantages in handling and space storability. Both OF_2 and B_2H_6 are storable in spacecraft, have compatible liquid range, and are hypergolic, with rather short ignition delay times, at sea level and at high altitudes. This Note discusses the results from some preliminary experiments designed to provide a qualitative understanding of the OF_2—B_2H_6 reaction. In these experiments, the partial pressures of OF_2 or B_2H_6 were 20 torr or less. The reacting mixture was studied by 1) observing it in Pyrex bulbs kept at ambient or lower temperatures, 2) determining gas composition vs time at ambient temperatures from infrared spectra, and 3) obtaining pressure-temperature relationships of an equimolar mixture at low pressures during a transient heat-up cycle (to 260°C) in a metal "reactor."

Experimental Methods and Results

The B_2H_6 (supplied by Callery Chemical Company) was purified, first, by being cooled to −195°C and pumped for H_2 removal. Then, after being warmed to −160°C (with an isopentane slush bath), it was pumped out and collected

Received September 15, 1969; revision received November 3, 1969. This paper presents the results of one phase of research carried out at the Jet Propulsion Laboratory, California Institute of Technology, under Contract NAS 7-100, sponsored by NASA.

* Senior Engineer.